NMR Docking of a Substrate into the X-ray Structure of the Asp-21 → Glu Mutant of Staphylococcal Nuclease[†]

David J. Weber,[‡,§] Andrew M. Libson,[⊥] Apostolos G. Gittis,[⊥] Michael S. Lebowitz,[‡] and Albert S. Mildvan*,[‡]

Departments of Biological Chemistry and Biophysics and Biophysical Chemistry, The Johns Hopkins University School of Medicine, 725 North Wolfe Street, Baltimore, Maryland 21205-2185

Received January 28, 1994; Revised Manuscript Received April 29, 1994[®]

ABSTRACT: To understand the structural basis of the 1500-fold decrease in catalytic activity of the D21E mutant of staphylococcal nuclease in which an aspartate ligand of the essential Ca^{2+} has been enlarged to glutamate, the conformation of the enzyme-bound substrate dTdA has been determined by NMR methods and has been docked into the X-ray structure of the D21E mutant (Libson, A. M., Gittis, A.G., & Lattman, E. E. *Biochemistry*, preceding paper in this issue) based on distances from the bound metal ion to dTdA and on intermolecular nuclear Overhauser effects from assigned aromatic proton resonances of Tyr-85, Tyr-113, and Tyr-115 to proton resonances of dTdA, using energy minimization to relieve small overlaps. Like the wild-type enzyme, the D21E mutant forms binary E–M and E–S and ternary E–M–S complexes with Ca^{2+}, Mn^{2+}, Co^{2+}, and La^{3+}. D21E enhances the paramagnetic effects of Co^{2+} on $1/T_1$ and $1/T_2$ of the phosphorus and on $1/T_1$ of four proton resonances of dTdA, and these effects are abolished by the binding of the competitive inhibitor 3′,5′-pdTp. From the paramagnetic effects of enzyme-bound Co^{2+} on $1/T_1$ of phosphorus and protons, with the use of a correlation time of 1.1 ps based on $1/T_1$ values at 250 and 600 MHz, five metal–nucleus distances and 11 lower limit metal–nucleus distances have been calculated. The Co^{2+} to ^{31}P distance of 4.1 ± 0.9 Å agrees with that found on the wild-type enzyme (Weber, D. J., Mullen, G. P., & Mildvan, A. S. (1991) *Biochemistry 30*, 7425–7437) and indicates at least 18% inner sphere phosphate coordination. Fourteen interproton distances and 109 lower limit interproton distances in dTdA in the ternary $D21E-La^{3+}-dTdA$ complex were determined by NOESY spectra at 50-, 100-, and 200-ms mixing times. Both the metal–nucleus and interproton distances were necessary to compute a narrow range of conformations for enzyme-bound dTdA. As on the wild-type enzyme, the conformation of dTdA on the D21E mutant is highly extended, with high-anti C-2′ endo conformations for the individual nucleosides. However, significant conformational differences are found in the torsional angles χ of dA ($\Delta\chi$ = 49 ± 3°), in γ of dT ($\Delta\gamma$ = 108 ± 30°) and in ζ of dT ($\Delta\zeta$ = 124 ± 38°). Despite these differences, in the NMR-docked ternary complex, the angle of nucleophilic attack, defined by the oxygen of an inner sphere water ligand of Ca^{2+}, the phosphorus, and the leaving 5′-deoxyadenosyl oxygen of dTdA of 139 ± 17° on D21E is very similar to that found on the wild-type enzyme (131 ± 16°) and is appropriate for inversion. The reaction coordinate distance from the water oxygen to the attacked phosphorus of 4.8 ± 0.5 Å agrees within error with that found on the wild-type enzyme (4.3 ± 0.5 Å) and is appropriate for an associative displacement at phosphorus. The catalytic residues, Arg-35 and Arg-87, interact similarly with the substrate on the D21E and wild-type enzymes. Hence, while other factors may contribute, the profound decrease in catalytic activity of the D21E mutant may result predominantly from the unavailability of Glu-43, due to its direct coordination by the metal ion, as found in the X-ray structure of the D21E–Ca^{2+}–3′,5′-pdTp complex (Libson, A., Gittis, A., & Lattman, E. E. (1993) *Biochemistry*, preceding paper in this issue). A catalytic role for Glu-43 is proposed in which this residue orients the attacking hydroxyl ligand on Ca^{2+}.

The mechanism of hydrolysis of DNA catalyzed by staphylococcal nuclease has been studied by a variety of methods including kinetics (Anfinsen *et al.*, 1971; Tucker *et al.*, 1978; Serpersu *et al.*, 1986, 1987; Hale *et al.*, 1993), X-ray diffraction (Cotton *et al.*, 1979; Loll & Lattman, 1989), NMR spectroscopy (Torchia *et al.*, 1989; Wang *et al.*, 1990;

Weber *et al.*, 1991a,b, 1992, 1993), site-directed mutagenesis (Serpersu *et al.*, 1986, 1987, 1989; Hibler *et al.*, 1987; Pourmotabbed *et al.*, 1990; Chuang *et al.*, 1993) and by the replacement of catalytic residues by unnatural amino acids (Judice *et al.*, 1993). A long unexplained observation is the unusually low catalytic activity of the D21E mutant of this enzyme in which the Asp-21 ligand of the essential Ca^{2+} is enlarged to a Glu (Serpersu *et al.*, 1987). We have previously used NMR docking to determine the structure of the ternary complexes of the wild-type enzyme with the substrate dTdA (Weber *et al.*, 1992) and with the potent competitive inhibitor 3′,5′-pdTp (Weber *et al.*, 1993). The structure at the active site of the wild-type enzyme as found by NMR docking of the substrate dTdA into the X-ray structure of the enzyme is shown in Figure 1A (Weber *et al.*, 1992). The NMR docking procedure is necessary in order to avoid a crystallographic artifact in which Lys-70* and Lys-71* from a neighboring enzyme molecule in the crystal lattice distort the conformation
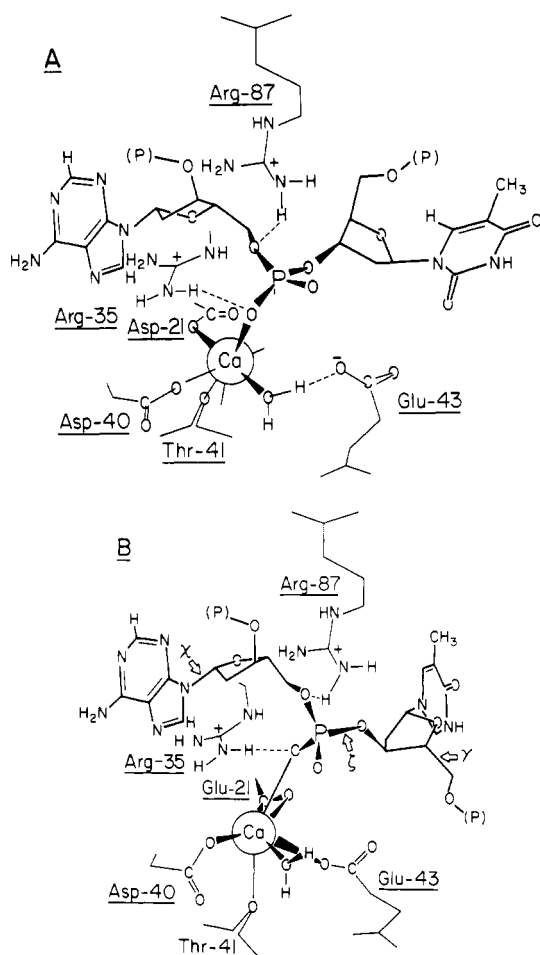
FIGURE 1: Structure at the active site of staphylococcal nuclease based on NMR docking of dTdA into the X-ray structure of the enzyme. (A) Wild-type enzyme (Loll & Lattman, 1989; Weber *et al.*, 1992). (B) D21E mutant. The bonds labeled χ, γ, and ζ are sites of conformational changes of the enzyme-bound substrate. The water ligand is seen as a vacancy in the X-ray structure (Libson *et al.*, 1994) but is detectable by NMR (Serpersu *et al.*, 1987).

of active site ligands (Loll & Lattman, 1989; Serpersu *et al.*, 1989; Weber *et al.*, 1993; Libson *et al.*, 1994).

The essential Ca^{2+} ion is coordinated by two strong monodentate carboxylate ligands, Asp-21 and Asp-40, and by the backbone carbonyl group of Thr-41 (Loll & Lattman, 1989) (Figure 1A). Glu-43 is positioned to accept a hydrogen bond from a water or hydroxyl ligand adjacent to the coordinated phosphoryl group of the substrate. Arg-35 and Arg-87 act as monofunctional hydrogen bond donors to the phosphoryl group in the substrate complex but are probably bifunctional in the transition state, as found in the X-ray structure of the enzyme–Ca^{2+}–3',5'–pdTp complex (Cotton *et al.*, 1979; Loll & Lattman, 1989) and in its refinement by NMR-docking which altered the conformation and some of the interactions of enzyme-bound 3',5'-pdTp, but preserved the bifunctional hydrogen bonds from Arg-35 and Arg-87 to the coordinated 5'-phosphate (Weber *et al.*, 1993; Chuang *et al.*, 1993).

While enlargement of Asp-40, one of the two strong ligands of Ca^{2+}, to Glu in the D40E mutant, resulted in only a 12-fold decrease in V_{max}, the same enlargement of the other strong ligand, Asp-21 to Glu in the D21E mutation, resulted in a 1500-fold decrease in V_{max} (Serpersu *et al.*, 1987). The 120-fold greater effect of enlarging Asp-21 was previously ascribed to overlap of Glu-21 with an adjacent water ligand on Ca^{2+} which might function as the attacking water, thereby

interfering with catalysis by approximation. However, this hypothesis is ruled out by the NMR-docked substrate complex (Figure 1A) which showed that a different water ligand, the one which is trans rather than adjacent to Asp-21, is in the best position to function as the attacking water (Weber *et al.*, 1992). The X-ray structure of the ternary D21E–Ca^{2+}–3',5'-pdTp complex reveals Glu-21 to be a bidentate ligand of Ca^{2+} which has moved the Ca^{2+} outward toward Glu-43 by 1.5 Å permitting Glu-43 to directly coordinate the metal ion (Figure 1B, Libson *et al.*, 1994). Although the position of the attacking water is not occupied in the X-ray structure, space at this position is detected (Libson *et al.*, 1994), and water proton relaxation and pulsed EPR measurements with the D21E–Mn^{2+}–3',5'-pdTp complex reveal one fast exchanging water ligand on the metal ion (Serpersu *et al.*, 1987, 1988).

Although its precise role is under discussion, Glu-43 is a catalytically important residue since its mutation results in 10^2- to 10^4-fold decreases in V_{max} (Hibler *et al.*, 1987). Hence, the 1500-fold decrease in V_{max} in the D21E mutant may result at least in part from the unavailability of Glu-43 due to its coordination by Ca^{2+}. The movement of Ca^{2+} resulting from the D21E mutation might also have affected V_{max} due to changes in the coordination and conformation of the enzyme-bound substrate. To examine these possibilities, we have studied the dTdA substrate complex of the D21E mutant by the NMR docking procedure, permitting a direct comparison with the same complex of the wild-type enzyme (Figure 1) (Weber *et al.*, 1992). The NMR docking procedure consists of four steps (Fry *et al.*, 1985; Weber *et al.*, 1992, 1993). 1. Determine the conformation of the enzyme-bound substrate (dTdA) by NMR measurements of metal–nucleus distances and interproton distances. 2. Measure distances from a paramagnetic reference point on the enzyme (Co^{2+}) to assigned proton resonances of the substrate. 3. Identify amino acid residues of the enzyme within 5 Å of the bound substrate by intermolecular NOEs from assigned proton resonances of the enzyme to those of the substrate. 4. Use the distances from steps 2 and 3 to position the proper conformation of the substrate into the X-ray structure of the enzyme, avoiding steric overlaps by energy minimization, if necessary.

A preliminary abstract of this work has been published (Weber *et al.*, 1994).

EXPERIMENTAL PROCEDURES

Materials. Solutions of the inhibitor 3',5'-pdTp (Pharmacia) were prepared utilizing an extinction coefficient (ϵ_{260}) of 9600 M^{-1} cm^{-1}. Before use, all buffer and inhibitor solutions were passed over Chelex-100 resin (Bio-Rad) to remove trace metals. Isolation of the mutant D21E staphylococcal nuclease from an engineered strain of *Escherichia coli* that carries the expression plasmid pFOG405 and purification to homogeneity were performed as described previously (Shortle & Lin, 1985; Serpersu *et al.*, 1986, 1987). All other reagents were of the highest purity commercially available.

Enzyme Assay. The enzymatic activity of the D21E mutant of staphylococcal nuclease was measured before and after all NMR experiments by observing the absorbance increase at 260 nm as DNA is hydrolyzed (Cuatrecasas *et al.*, 1967a,b). Protein concentration was determined by absorbance at 280 nm ($\epsilon^{0.1\%} = 0.93$) at neutral pH (Dunn *et al.*, 1973; Tucker *et al.*, 1978, 1979) or in the presence of nucleotides by the method of Bradford (1976) with the D21E mutant staphylococcal nuclease as the standard. The specific activity of the enzyme was found to be 1.5 units/mg, and the enzyme retained at least 94% of its activity after prolonged NMR studies.

Binding Studies. The concentration of free Mn^{2+} in a mixture of free and bound Mn^{2+} was determined by electron paramagnetic resonance (Cohn & Townsend, 1954) with a Varian E4 EPR spectrometer. These data were supplemented by studies of bound Mn^{2+} in the same solution by measuring the longitudinal relaxation rates of water protons at 24.3 MHz as described previously (Mildvan & Engle, 1972) with use of a Seimco pulsed NMR spectrometer and a $180°-\tau-90°$ pulse sequence (Carr & Purcell, 1954; Mildvan & Engle, 1972). The observed enhancement of the longitudinal relaxation rate is defined as $\epsilon^* = (1/T_{1p}^*)/(1/T_{1p})$, where $1/T_{1p}$ is the paramagnetic contribution to the relaxation rate in the presence (*) and absence of enzyme (Mildvan & Engle, 1972). The stoichiometry of Mn^{2+} ions bound to the D21E mutant enzyme (n), the dissociation constant (K_D), and the enhancement factor of the binary enzyme–Mn^{2+} complex (ϵ_b) were previously reported as was the dissociation constant of the binary enzyme–Ca^{2+} complex, obtained by competition with Mn^{2+} (Serpersu et al., 1987). The binding of Mn^{2+} to the enzyme–dTdA complex was monitored by EPR and by changes in $1/T_{1p}$ of water protons to provide the dissociation constant of Mn^{2+} from the ternary D21E–Mn^{2+}–dTdA complex. The binding of dTdA to the D21E–Mn^{2+} complex was monitored by changes in $1/T_{1p}$ of water protons and analyzed as previously described (Reed et al., 1970; Mildvan & Engle, 1972) to give dissociation constants and enhancement factors of ternary D21E–Mn^{2+}–dTdA complexes. The dissociation constants of Ca^{2+}, Co^{2+}, and La^{3+} from their binary and ternary D21E complexes were determined by competition experiments with Mn^{2+}, monitoring the bound Mn^{2+} by $1/T_{1p}$ of water protons and the free Mn^{2+} by EPR, and the data were analyzed as previously described (Serpersu et al., 1986; Weber et al., 1990, 1991b).

^{31}P Relaxation Rate Measurements of dTdA. To determine the paramagnetic effects of enzyme-bound Co^{2+} on the relaxation rates of the phosphorus nucleus of dTdA bound to D21E staphylococcal nuclease, 2.0-mL samples were prepared containing 10 mM TES,[1] pH 7.4, 30 mM NaCl, 20% ^2H_2O for field/frequency locking, 4.0 mM dTdA, and 0.40 mM D21E staphylococcal nuclease. The solution was then titrated with $CoCl_2$, and the increase in longitudinal ($1/T_1$) and transverse ($1/T_2$) relaxation rates of the phosphorus resonance of dTdA were measured. Following the titration with $CoCl_2$, dTdA was displaced from the ternary enzyme–Co^{2+}–dTdA complex with the potent competitive inhibitor $3',5'$-pdTp, permitting the measurement of the outer sphere contribution to $1/T_{1p}$ and $1/T_{2p}$ of dTdA.

The paramagnetic effects on dTdA were analyzed by plotting the increase in relaxation rates as a function of Co^{2+} concentration. Subtraction of the residual outer sphere effect measured after displacing dTdA by $3',5'$-pdTp then gives the observed $1/T_{1p}$ or $1/T_{2p}$, respectively. Similarly, paramagnetic effects on $1/T_1$ and $1/T_2$ in the binary Co^{2+}–dTdA complex were analyzed in a control experiment in which dTdA alone was titrated with Co^{2+}. The effect of the binary Co^{2+}–dTdA complex ($1/fT_{1p}$) is subtracted from the observed effect ($1/T_{1p}$)$_{obs}$ in the ternary system and normalized by the concentrations of ternary complex (EMS) and total substrate (S_T) to yield ($1/fT_{1p}$)$_{corr}$, the corrected relaxation rate in the

cation	K_D	K_A'	K_S	K_3	K_2
Mn^{2+}	397 ± 40[b]	363 ± 13	10720 ± 2680	9802 ± 2450	17.3 ± 5
Ca^{2+}	997 ± 103[b]	922 ± 5	10720 ± 2680	9914 ± 2676	43.9 ± 12
Co^{2+}	1218 ± 239	1964 ± 404	10720 ± 2680	17286 ± 6396	93.6 ± 39
La^{3+}	235 ± 52	228 ± 73	10720 ● 2680	10400 ± 4554	10.9 ± 7

[a] The dissociation constants of the ternary and of the relevant binary complexes of enzyme (E), metal (M), and ligands (L) are defined as follows: $K_1 = [M]/[L]/[M - L]$; $K_D = [E][M]/[E - M]$; $K_2 = [E][M - L]/[E - M - L]$; $K_a' = [M][E - L]/[E - M - L]$; $K_3 = [E - M]/[E - M - L]$; $K_S = [E][L]/[E - L]$. Note that $K_1K_2 = K_3K_D = K_a'K_s$. For dTdA $K_1 = 0.225$ M is estimated on the basis of measurements of Mn^{2+} – ApU (Bean et al., 1977). The enhancement factor (ϵ_T) of the ternary D21E–Mn^{2+}–dTdA complex is 17.4 ± 0.6, similar to that of the wild-type enzyme (18.3 ± 1.8). [b] The value given and the stoichiometry for Mn^{2+} binding in the binary E–Mn^{2+} complex of 0.95 ± 0.08 are based on EPR and $1/T_{1P}$ of water proton titrations done previously (Serpersu et al., 1987).

ternary complex, using the equation:

$$(1/fT_{1P})_{corr} = \frac{(1/T_{1P})_{obs} - (MS)/(S_T)(1/fT_{1P})_b}{(EMS)/(S_T)}$$

The concentrations of the binary metal–substrate complex and the ternary enzyme–metal–substrate complex were computed by use of the measured dissociation constants of the relevant binary and ternary complexes (Table 1).

Proton-decoupled ^{31}P NMR spectra were obtained at 101.25 MHz using 12-bit analog to digital conversion, collecting 16K data points over a spectral width of 5000 Hz with an acquisition time of 1.64 s. Routine spectra were acquired by collecting 16–128 transients, with an 18-s delay to obtain fully relaxed spectra ($>5T_1$). The longitudinal relaxation rates ($1/T_1$) of the ^{31}P resonance were measured by the saturation–recovery method, which permitted shorter recycle times. Transverse relaxation rates ($1/T_2$) were determined from the widths of resonances of half-height ($\Delta\nu_{1/2}$), where $1/T_2 = \pi\Delta\nu_{1/2}$. Phosphorus chemical shifts are referenced with respect to 85% H_3PO_4.

Proton Relaxation Rate Measurements of dTdA. To determine the paramagnetic effects of enzyme-bound Co^{2+} on the relaxation rates of the proton resonances of dTdA bound to the D21E mutant of staphylococcal nuclease, 0.5-mL samples were prepared in D_2O containing 2.1 mM deuterated Tris–HCl, pD 7.4 (pH* 7.0), 40 mM NaCl, 15.0 mM dTdA, and 1.5 mM of the D21E mutant of staphylococcal nuclease. The resulting sample was titrated with $CoCl_2$, and the increases in longitudinal ($1/T_1$) and transverse ($1/T_2$) relaxation rates of proton resonances of dTdA were measured. These data were corrected for outer sphere relaxation and were analyzed as described above for phosphorus to obtain ($1/fT_{1p}$)$_{corr}$ and ($1/fT_{2p}$)$_{corr}$. The correlation time τ_c for electron nuclear dipolar interaction in the ternary enzyme–Co^{2+}–dTdA complex was determined by measuring the frequency dependence of ($1/fT_{1p}$)$_{corr}$ of the AH8 proton of dTdA at both 250 and 600 MHz. Evaluation of τ_c from frequency dependent $1/fT_{1p}$ values and distance calculations were carried out as described earlier (Mildvan & Gupta, 1978; Mildvan et al., 1979; Serpersu et al., 1989).

Proton NMR spectra were collected at 250 and 600 MHz on Bruker AM 250 and AM 600 NMR spectrometers by collecting 16K data points over a spectral width of 3356 or 8064 Hz for acquisition times of 2.44 and 1.01 s, respectively. Fully relaxed spectra were obtained with an 18-s delay ($>5T_1$), and 16–128 transients were acquired for all spectra. The

longitudinal relaxation rates $(^1/T_1)$ of the proton resonances were measured by the nonselective saturation–recovery method, and the transverse relaxation rates were derived from the widths of the resonances at half-height, as described for the ^{31}P experiments. All proton chemical shifts are reported with respect to external DSS.

Two-Dimensional NOE Experiments. NOESY spectra (Jeener et al., 1979; Kumar et al., 1980) were acquired at 600 MHz in D_2O. The samples contained 2.47 mM D21E mutant staphylococcal nuclease, 8.65 mM dTdA, 36.7 mM NaCl, 2.40 mM LaCl$_3$, 0.05 mM EGTA, and 1.66 mM deuterated Tris–DCl, pD 7.40 (pH* 7.0) in a total volume of 0.545 mL. Samples were examined at three mixing times of 50, 100, and 200 ms, and the mixing times were randomized by $\sim10\%$ to eliminate COSY cross-peaks. All spectra were acquired in the phase-sensitive mode with the use of time-proportional phase incrementation (TPPI) (Marion & Wüthrich, 1983). Optimization of the receiver phase was performed to reduce base-line roll and to minimize phase correction in F2. The parameters for acquisition of NOESY spectra included a 2-s relaxation delay, a 0.254-s acquisition time, an 8064-Hz spectral width, 4096 time domain points in F2, 1024 time domain points in F1, and a filter width of 30 kHz.

NOESY data were processed on an Aspect 3000 computer, with Bruker software and on a Personal IRIS (Silicon Graphics, Inc.), utilizing the software FELIX (Hare, Inc.) with no significant differences. NMR data processed by Bruker software were multiplied by a $\pi/2$ shifted squared sine-bell prior to Fourier transformation in F2. Linear base-line correction in F2 was done throughout the entire spectrum, and the F1 dimension was Fourier transformed with zero filling to 2K points. The resulting NOE crosspeaks were examined both by volume integration routines and by measuring the area of optimal slices as described previously (Weber et al., 1991b). To obtain interproton distances, the integrated peaks were analyzed by comparing their initial slopes versus mixing time (Wüthrich, 1986; Baleja et al., 1990) or by extrapolation of distances to zero mixing time (Baleja et al., 1991) using the reference distance from H$_1'$ to H$_2''$ of 2.37 $\pm$ 0.10 Å, as previously described (Weber et al., 1991b). The NOESY spectra were also used to confirm the resonance assignments of residues Tyr-85, Tyr-113, and Tyr-115 in the ternary D21E–La^{3+}–dTdA complex in comparison with those of the same complex of the wild-type enzyme (Weber et al., 1992). Intermolecular NOEs from the aromatic protons of these tyrosine residues to protons of dTdA were measured on the 50-ms NOESY spectra.

Modeling Studies. The conformation of enzyme-bound dTdA was initially explored by building skeletal models and adjusting them to accommodate measured distances, bond distances, and van der Waals radii. Utilizing the interproton distances and the metal–nucleus distances, only one structure could accommodate all distance constraints. To independently determine the range of conformations of dTdA within the error limits of the internuclear distance data, a computer search procedure, D-Space (Hare Research, Inc.), was utilized. In this approach, atomic coordinates of dTdA were initially randomized by 20 Å movements of atoms in all directions, followed by annealing in four-dimensional space (to avoid local minima). For the enzyme–metal–dTdA ternary complex, 50 searches were performed yielding seven acceptable structures based on their consistency with all covalent, van der Waals, and angle constraints and with measured distances within their experimental errors.

Docking the Metal–dTdA Complex into the X-ray Structure. As previously described for the wild-type enzyme (Weber et al., 1992), the structural coordinates for the best fit enzyme-bound metal–dTdA complex obtained with the D21E mutant were combined with the 1.95 Å X-ray coordinates of the ternary D21E–Ca^{2+}–3',5'–pdTp complex (Libson et al., 1994). The metal–dTdA complex was positioned manually into the active site of the enzyme using the software program CHAIN (Sack, 1988) on a Silicon Graphics IRIS work station. Initially, the metal of the metal–dTdA complex was superimposed onto the Ca^{2+} position in the X-ray structure, and subsequently the dTdA was oriented taking into consideration the intermolecular NOE constraints from protons of dTdA to assigned side chain protons of Tyr-85, 113, and 115 of the enzyme. As with the wild-type enzyme (Weber et al., 1992) several orientations of the substrate were explored manually due to overlaps of the chemical shifts of the aromatic proton resonances of Tyr-85 and Tyr-113. However, only one orientation could be found which simultaneously satisfied all of the intermolecular NOEs, the position of the metal ion, and the conformations of the enzyme and substrate. To relieve residual van der Waals overlaps and to optimize the structure, the manually docked D21E–metal–dTdA complex was subjected to 500 cycles of restrained Powell energy minimization using the program X-PLOR (Brünger, 1990) on a Convex C220 computer as previously described (Weber et al., 1992, 1993) using the experimental errors in all measured distances as restraints. No significant changes in the structure occurred when the number of cycles was increased to 700. When the docking procedure was repeated with the most different acceptable conformation for the enzyme-bound metal–dTdA complex, a very similar final structure of the ternary complex was obtained.

RESULTS

Thermodynamics of the D21E–Metal–dTdA Binary and Ternary Complexes. To quantitatively interpret the relaxation rates of enzyme-bound dTdA, the dissociation constants of the complexes studied by NMR are required. The Mn^{2+} complexes are easily monitored by EPR and by $^1/T_{1p}$ of water protons (Serpersu et al., 1986), and the dissociation constants of Ca^{2+}, Co^{2+}, and La^{3+} are determined by competition studies with Mn^{2+}.

(A) Titration of D21E–dTdA with Mn^{2+}. The dissociation constant for Mn^{2+} from the ternary D21E–Mn^{2+}–dTdA, K_A', was determined in a titration of Mn^{2+} into a solution of D21E and dTdA, measuring the free Mn^{2+} by EPR and the bound Mn^{2+} by its effects on $^1/T_1$ of water protons. Scatchard plots of both the EPR data (Figure 2A) and the $^1/T_{1p}$ data (not shown) yielded 0.92 $\pm$ 0.02 tight binding sites for Mn^{2+} with an average K_A' value of 363 $\pm$ 13 μM by the two methods (Table 1).

Unlike the ternary complex of the wild-type enzyme in which the presence of dTdA slightly lowers the affinity of the enzyme for Mn^{2+} by a factor of 1.35 $\pm$ 0.15 (Weber et al., 1991b), with the D21E mutant the presence of dTdA has no effect on Mn^{2+} binding since the ratio of K_A'/K_D is 0.91 $\pm$ 0.10 (Table 1), indicating a difference in the interaction of the metal ion with the enzyme in the D21E mutant.

(B) Displacement of Mn^{2+} by Ca^{2+}, Co^{2+}, and La^{3+} in Binary and Ternary Complexes of the D21E Mutant Staphylococcal Nuclease. The dissociation constant of the binary Mn^{2+} complex of the D21E mutant staphylococcal nuclease has previously been determined by EPR and by $^1/T_{1p}$ of water protons to be 397 $\pm$ 40 μM (Serpersu et al., 1987).
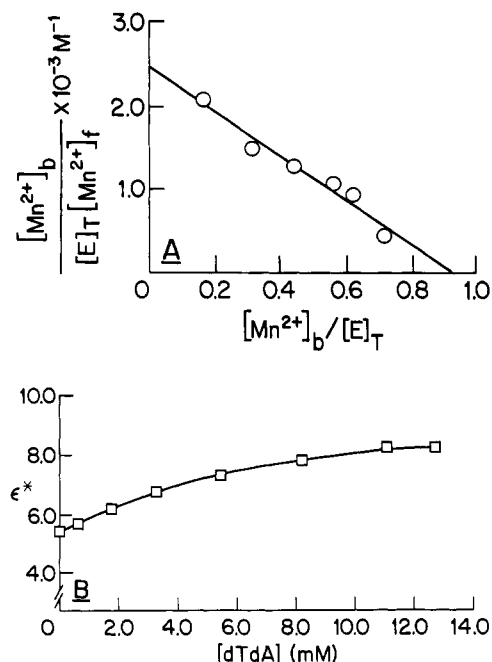
FIGURE 2: Mn^{2+} and dTdA binding by staphylococcal nuclease. (A) Scatchard plot of a titration of D21E staphylococcal nuclease with Mn^{2+} in the presence of dTdA. The solution contained 0.870 mM D21E enzyme and 8.89 mM dTdA. (B) Titration of the enzyme–Mn^{2+} binary complex with dTdA, measuring the changes in enhancement ϵ^* of the paramagnetic effects of Mn^{2+} on $1/T_{1P}$ of water protons. The solution contained 0.580 mM D21E enzyme with 0.113 mM $MnCl_2$. Also present was 40 mM Tris–Cl, pH 7.4. The nucleotide was added from concentrated stock solution which also contained all other components of the titration at the same concentrations. The solid curve is computed utilizing the equilibrium constants given in Table 1.

Titrations of the binary D21E–Mn^{2+} complex with Co^{2+} and La^{3+} and the ternary D21E–Mn^{2+}–dTdA complex with Ca^{2+}, Co^{2+}, and La^{3+} were carried out by measuring the decrease in $1/T_{1p}$ of water protons (Figure 3) resulting from the displacement of Mn^{2+} by the competing metal. This displacement was independently monitored by the increase in free Mn^{2+} as measured by EPR, indicating that in all cases Co^{2+}, Ca^{2+}, and La^{3+} compete for a single common Mn^{2+} site in both binary and ternary complexes as previously observed for the wild-type enzyme (Weber *et al.*, 1991b). The affinity for metal ions varies only slightly in the binary (5.5-fold) and ternary (8.6-fold) complexes when the weakest Co^{2+} complexes are compared to the strongest La^{3+} complexes (Table 1).

The catalytically active ternary Ca^{2+} complex was shown to bind Ca^{2+} only 4-fold weaker than La^{3+} when the K_A' values are compared (Figure 3, Table 1). Interestingly, the dissociation of Ca^{2+} from the active enzyme–Ca^{2+}–dTdA ternary complex for wild type enzyme ($K_A' = 1780 \pm 150$; Weber *et al.*, 1991b) is 2-fold weaker than the dissociation constant from the corresponding D21E mutant complex (Table 1). In all Ca^{2+} titrations, during the course of the experiment, less than 5% of the dTdA was hydrolyzed, as determined by thin-layer chromatography.

(C) Titration of the Enzyme–Mn^{2+} Complex with dTdA. Solutions of D21E and Mn^{2+} were titrated with dTdA and monitored by changes in enhancement (ϵ^*) of $1/T_{1p}$ of water protons (Mildvan & Engle, 1972) to determine K_3, the dissociation of dTdA from the ternary D21E–Mn^{2+}–dTdA complex. Such titrations, fit by computed curves (Figure 2B), yield the average K_3 values shown in Table 1. The computer fitting of nucleotide titrations also required values for K_S, the dissociation constant of the binary enzyme nucleotide complex.
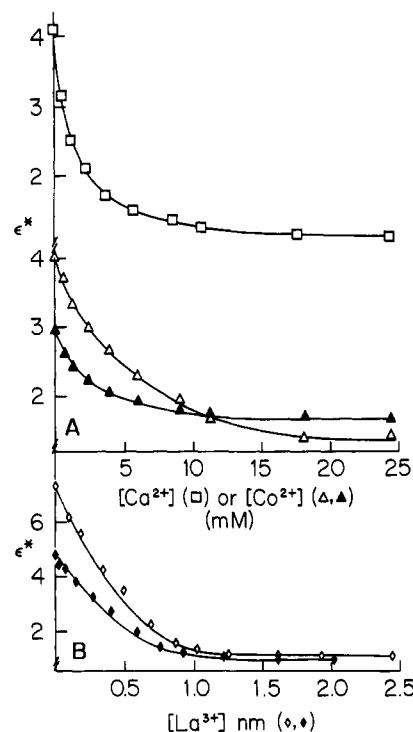

FIGURE 3: Displacement of Mn^{2+} by Ca^{2+}, Co^{2+}, or La^{3+} from binary and ternary complexes of D21E mutant staphylococcal nuclease monitored by changes in enhancement (ϵ^*) of the effects of Mn^{2+} on $1/T_1$ of water protons. (A) Displacement of Mn^{2+} by Ca (□) from ternary enzyme–Mn^{2+}–dTdA and displacement of Mn^{2+} by Co^{2+} from binary enzyme–Mn^{2+} (▲) and ternary enzyme–Mn^{2+}–dTdA complex (△) of D21E mutant enzyme. The solutions contained 277.5 μM D21E with 112.7 μM $MnCl_2$ and 3.81 mM dTdA (□), 347.3 μM D21E, and 112.7 μM $MnCl_2$ (▲), and 347.3 μM D21E with 112.7 μM $MnCl_2$ and 3.81 mM dTdA (△). (B) Displacement of Mn^{2+} by La^{3+} from binary enzyme–Mn^{2+} (◆) and ternary enzyme–Mn^{2+}–dTdA (◇) complexes of D21E mutant staphylococcal nuclease. The solutions contained 243 μM D21E with 59.5 μM $MnCl_2$ and 4.92 mM dTdA (◇) and 486 μM D21E with 59.5 μM $MnCl_2$ (◆). In the Co^{2+} titrations the solutions contained 40 mM TES–Na^+, pH 7.4, and in all other titrations the solutions contained 40 mM Tris–HCl, pH 7.4. For all titrations the competing metal ion (Co^{2+}, Ca^{2+}, or La^{3+}) was added from concentrated stock solutions that also had the other components of the titration at the same final concentrations.

Although determined indirectly by such analysis, the resulting K_S value ($10\,720 \pm 2680$ μM) was consistent with data from dTdA titrations at three Mn^{2+} concentrations ranging from 113.4 to 226.8 μM at a constant enzyme concentration (580 μM). By comparing K_3 and K_S, the binding of dTdA is shown to be unaffected by the presence of the metal ion, a finding consistent with the lack of an effect of dTdA on Mn^{2+} binding to the enzyme. In contrast, a comparison of K_2 and K_3 of the wild-type enzyme indicates that metal ions slightly weaken the binding of dTdA (Weber *et al.*, 1991b).

Paramagnetic Effects of Enzyme-Bound Co^{2+} on Relaxation Rates of Proton and Phosphorus Resonances of dTdA. (*A) Proton Relaxation Studies.* Titrations of the substrate dTdA with $CoCl_2$ measuring $1/T_1$ of the proton resonances of dTdA in the absence or presence of the D21E mutant enzyme show that the enzyme enhances the paramagnetic effects of Co^{2+} on $1/T_1$ of the deoxyadenosine protons of dTdA, AH_8, and AH_2 (Figure 4A,B) and the thymidine protons TH_2'' and TH_3' (Figure 4A). The enhancement factors, obtained from the ratios of slopes in the titration curves of Figure 4 to those in control titrations lacking enzyme (data not shown), were 5.25 and 2.09 for the adenine H_8 and H_2, respectively, and 2.50 and 1.46 for the thymidine H_3' and $H2''$, respectively. Displacement of dTdA from the ternary D21E–Co^{2+}–dTdA
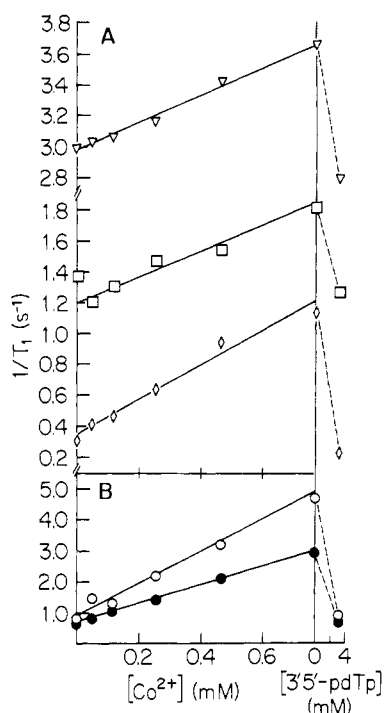
FIGURE 4: Paramagnetic effects of Co^{2+} on proton resonances of dTdA at 250 MHz and the frequency dependence of the effects of AH_8 proton at 250 and 600 MHz. (A) $1/T_1$ of proton resonances of dTdA as a function of $[Co^{2+}]$, and displacement of dTdA from the enzyme by the competitive inhibitor 3′,5′-pdTp for the protons ($\diamond$) AH_2, ($\square$) TH_3', and ($\triangledown$) TH_2'' of dTdA. (B) Frequency dependence of the paramagnetic effects of Co^{2+} ions on the AH_8 proton resonance of dTdA at 250 MHz ($\bigcirc$) and 600 MHz ($\bullet$). The solutions contained 1.5 mM D21E mutant staphylococcal nuclease, 15.0 mM dTdA, 40 mM NaCl, and 1.53 mM deuterated Tris–DCl, pD = 7.48, 25 °C. Displacement of dTdA from D21E enzyme was with 3′,5′-pdTp at a final concentration of 3.1 mM.

complex by the competitive inhibitor 3′,5′-pdTp abolished the paramagnetic effects on the thymidine H_2'' and the adenine H_2 proton resonances and significantly decreased the paramagnetic effects on the thymidine H_3' and adenine H_8 proton resonances (Figure 4). The outer sphere contributions to $1/T_{1p}$, thus determined, were used to correct the relaxation rates for the distance calculations. The concentration of 3′,5′-pdTp (600 ± 100 μM) that gave half-maximal displacement of dTdA was comparable to that predicted (300 ± 200 μM) on the basis of the dissociation constants for the ternary Co^{2+} complexes of dTdA (Table 1) and 3′,5′-pdTp (Serpersu *et al.*, 1988).

(B) Phosphorus Relaxation Studies. The substrate dTdA was titrated with Co^{2+} in the presence (Figure 5) and absence of the D21E mutant enzyme (not shown) monitoring $1/T_1$ and $1/T_2$ of the phosphorus resonance of dTdA. The presence of the enzyme enhanced the paramagnetic effects of Co^{2+} on $1/T_1$ and $1/T_2$ of the phosphorus of dTdA by factors of 3.2 and 4.0, respectively. Displacement of dTdA was achieved by titrating with the potent competitive inhibitor 3′,5′-pdTp and measuring the decreases in $1/T_2$ and $1/T_1$ of the phosphorus resonance (Figure 5). Since the total paramagnetic effect was abolished by this titration, the residual outer sphere contribution to the relaxation rate of phosphorus is negligible. The concentration of 3′,5′-pdTp (130 ± 20 μM) that gave half-maximal displacement of dTdA from the ternary Co^{2+} complex was similar to that predicted (100 ± 67 μM) on the basis of the dissociation constants for the ternary Co^{2+} complexes of dTdA (Table 1) and 3′,5′-pdTp (Serpersu *et al.*, 1988).

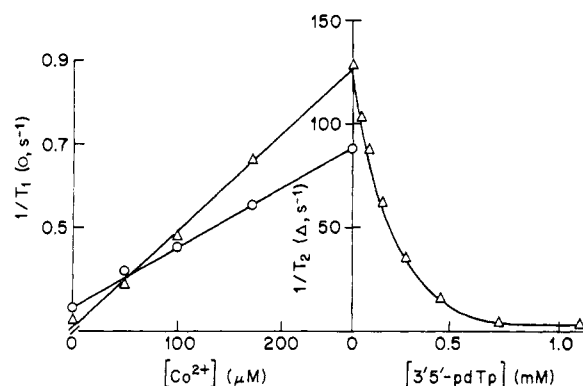FIGURE 5: Paramagnetic effects of Co^{2+} on $1/T_1$ ($\bigcirc$) and $1/T_2$ ($\triangle$) of the phosphorus resonance of dTdA at 101.25 MHz. The solution contained 0.400 mM D21E mutant staphylococcal nuclease, 4.0 mM dTdA, 30 mM NaCl, 20% ^2H_2O for field frequency locking, and 10 mM TES–Na⁺, pH 7.4, at 25 °C. Displacement of dTdA from the enzyme was with 3′,5′-pdTp titrated to a final concentration of 1.10 mM. At this concentration of pdTp, T_1 returned to its initial value found at $[Co^{2+}]$ = 0.

Cobalt to Phosphorus and Cobalt to Proton Distances in the Ternary Enzyme–Co^{2+}–dTdA Complex. The concentrations of Co^{2+} in the binary Co^{2+}–dTdA and ternary D21E–Co^{2+}–dTdA complex were calculated from the six dissociation constants listed in Table 1, permitting an evaluation of the normalized relaxation rates $(1/fT_{1p})_{corr}$ and $(1/fT_{2p})_{corr}$ for protons and phosphorus in each ternary complex (see the Experimental Procedures). The $(1/fT_{2p})_{corr}$ value for phosphorus (3.9×10^4 s⁻¹, Table 2) sets a lower limit to the rate constant for dissociation of dTdA from the ternary complex. From this value and K_3 (Table 1), a lower limit rate constant for the binding of dTdA of 3.7×10^6 M⁻¹ s⁻¹ is obtained. These values, which are several orders of magnitude larger than any $(1/fT_{1p})_{corr}$ value establish that dTdA is in the fast exchange regime (Mildvan & Engle, 1972; Mildvan & Gupta, 1978). Thus, the values of $(1/fT_{1p})_{corr}$ from the paramagnetic effects of Co^{2+} in the ternary D21E–Co^{2+}–dTdA complex are suitable for distance calculations. The correlation time, τ_c, another parameter required for distance calculations, was determined from the frequency dependence of $(1/fT_{1p})_{corr}$ of the AH_8 proton at 250 and 600 MHz (Mildvan & Engle, 1972; Serpersu *et al.*, 1988; Weber *et al.*, 1991b) (Figure 4B). Assuming τ_c to be independent of frequency over the range 250–600 MHz, the ratio of fT_{1p} (600 MHz)/fT_{1p} (250 MHz) of 1.58 ± 0.02 allows the calculation of τ_c to be 1.10 ± 0.05 ps. The alternative assumption, that τ_c showed a maximal frequency dependence over this range, was inconsistent with the ratio of fT_{1p} values measured. This correlation time, which is dominated by the longitudinal electron spin relaxation time of Co^{2+} was used in all distance calculations (Table 2). It is somewhat shorter than the τ_c value found by the same methods for the wild-type enzyme (1.64 ● 0.06 ps, Weber *et al.*, 1991b) indicating a change in the environment of the metal ion on the D21E mutant. In cases where paramagnetic enhancements were not detected or where large outer-sphere contributions were observed, lower limit distances were calculated from experimental error levels of the $1/T_{1p}$ values (Table 2).

With the D21E mutant, the Co^{2+} to phosphorus distance (4.1 ± 0.9 Å), is unchanged from that found in the wild-type complex and lies between that expected for direct phosphate coordination (3.31 ± 0.02 Å) and a second sphere complex with an intervening water molecule (4.75 ± 0.02 Å) (Serpersu *et al.*, 1989). The value of 4.1 Å is consistent with either a distorted inner-sphere phosphoryl complex or the rapid averaging of 18% inner-sphere and 82% second-sphere

Table 2: Distances from Co^{2+} to Protons and Phosphorus of dTdA in the D21E–Co^{2+}–dTdA Complex of Staphylococcal Nuclease

nucleus	δ^a (ppm)	$1/fT_{1P,corr}{}^b$ (s^{-1})	r^c (Å)	nucleus	δ^a (ppm)	$1/fT_{1P,corr}{}^b$ (s^{-1})	r^c (Å)
AH$_8$	8.35	391.5 ± 46.6	4.5 ± 1.0	TH$_6$	7.26	≤124.9	≥5.5
AH$_2$	8.18	92.0 ± 6.9	7.5 ± 1.7	TCH$_3$	1.82	≤60.9	≥6.2
AH$_1'$	6.37	≤45.8	≥6.5	TH$_1'$	5.96	≤29.4	≥7.0
AH$_2'$	2.81	≤139	≥5.4	TH$_2'$	1.63	≤112.1	≥5.6
AH$_2''$	2.56	≤547.0	≥4.3	TH$_2''$	2.20	35.6 ± 6.4	6.8 ± 1.6
AH$_4'$	4.14	≤849	≥4.0	TH$_3'$	4.60	63.4 ± 38.7	6.6 ± 1.4
AH$_5'$H$_5''$	4.03	≤100.8	≥5.7	TH$_4'$	4.00	≤647.0	≥4.3
P	0.33	127.3 ± 18.0^d	4.1 ± 0.9	TH$_5'$H$_5''$	3.61	≤282.7	≥4.8

^{a} ±0.02 ppm from external DSS (protons) or from 85% H_3PO_4 in 20% ^2H_2O (phosphorus). ^{b} $1/fT_{1P}$ values were obtained as described in the text. ^{c} Distances were obtained as described in the text. The τ_c was determined as 1.10 ± 0.5 ps from the frequency dependence of $1/fT_{1P,corr}$ of AH$_8$ (Figure 4B). Errors in r include contributions from errors in $1/fT_{1P}$ and τ_c and on the assumption that the C values used have a g value for high-spin Co^{2+} of 4 ± 2. The C values used are 895 ± 125 for Co^{2+}–proton distances and 662 ± 93 for Co^{2+}–^{31}P interactions. Errors are shown in the absolute distances, which include a 14% contribution from the anisotropic g values of Co^{2+} and 5–7% contributions due to experimental errors in measurements of $1/fT_{1P}$, τ_c, and the thermodynamic parameters. If the g tensor were the same in all complexes, the errors in the relative distances would be 5–7%. ^{d} $1/T_2$ values were calculated as $\pi\Delta\nu_{1/2}$. The $(1/fT_{2P})_{corr}$ of P is 39 340 ± 987 as determined by a least-squares fit of $1/T_2$ vs $[Co^{2+}]$ (Figure 5) and is corrected for binary dTdA–Co^{2+} contributions as described for $1/fT_{1P,corr}$. Since $1/fT_{2P,corr} \gg 1/fT_{1P,corr}$ fast substrate exchange assumptions are valid, eliminating τ_M, the lifetime of the complex, from the Solomon–Bloembergen equation for $(1/fT_{1P})_{corr}$ (Mildvan & Engle, 1972; Mildvan & Gupta, 1978; Weber et al., 1991b).

coordination. Alternatively, the 4.1 Å distance, which is more appropriate for the activating Ca^{2+} ion, may result from a less precisely defined site for smaller metal ions such as Co^{2+} on both the wild-type and D21E enzymes.

Four distances from protons to Co^{2+} range from 4.5 to 7.5 Å (Table 2) and 11 lower limit distances, together with the phosphorus to Co^{2+} distance, lead to an extended conformation of dTdA bound to D21E, as previously found for the wild-type enzyme (Weber et al., 1991b). However, a unique conformation could not be obtained from these few constraints. Since additional constraints could be obtained by measurements of interproton distances by the nuclear Overhauser effect, ambiguities in the enzyme-bound dTdA were resolved by this method.

Intramolecular Nuclear Overhauser Effects on Enzyme-Bound dTdA. To prevent hydrolysis of the substrate, dTdA, the diamagnetic metal La^{3+} was substituted for Ca^{2+} in the ternary D21E–metal–dTdA complex. It is clear that La^{3+} occupies the Ca^{2+} site from the competition studies in which both La^{3+} and Ca^{2+} displace Mn^{2+} which occupies the active site (Figure 3; Table 1). Slices along F1 of a phase-sensitive NOESY spectrum of the D21E–La^{3+}–dTdA complex (t_m = 100 ms) are shown in Figure 6. In spectrum A the AH$_8$ resonance of enzyme-bound dTdA is on the diagonal, giving rise to the negative NOEs displayed, while in spectrum B the TH$_6$ proton of enzyme-bound dTdA is on the diagonal. The negative signs of the NOEs of dTdA establish these to come only from the enzyme-bound substrate. In the absence of enzyme, NOEs of dTdA are positive and appear much more slowly (not shown) as is generally observed for small molecules (Rosevear et al., 1983; Ferrin and Mildvan, 1985). This was independently confirmed by displacement experiments with 3',5'-pdTp which eliminated the negative NOEs arising from enzyme-bound dTdA. Negative NOEs from enzyme-bound 3',5'-pdTp then appeared.

To determine interproton distances, NOESY spectra were collected at three mixing times (50, 100, and 200 ms) to obtain data which could be corrected for spin diffusion. The NOESY spectrum at the lowest (50 ms) mixing time was repeated since these measurements are critical in extrapolations and they have the lowest signal to noise ratio. In one method, NOE buildup curves (NOE intensity vs mixing time) were plotted and the initial slope (σ) of a reference NOE (i.e., H$_1'$ ↔ H$_2''$) was compared to that of the NOE of interest. Using the relationship $r = 2.37/(\sigma_{xx}/\sigma_{H1'\sigma H2''})^{1/6}$, 14 intramolecular distances were calculated for enzyme-bound dTdA
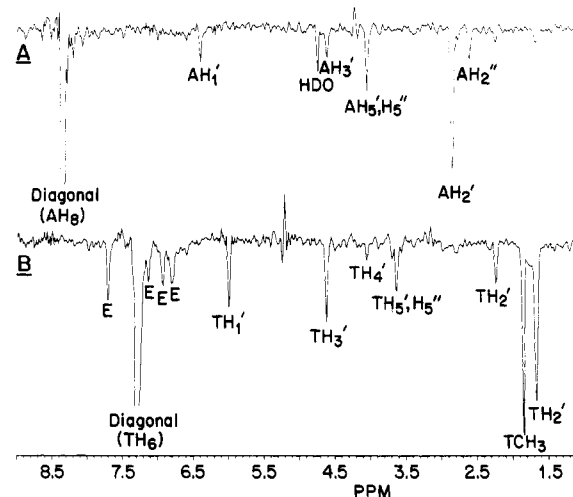

FIGURE 6: Representative slices along F1 from a two-dimensional nuclear Overhauser effect (NOESY) spectrum at 600 MHz (t_m = 100 ms) of the D21E–La^{3+}–dTdA ternary complex of staphylococcal nuclease. (A) NOEs arising from the AH$_8$ proton (8.3 ppm) and (B) TH$_6$ proton (7.3 ppm) of dTdA. The peaks labeled E are NOEs from protons of the enzyme.

(Table 3). The same data were analyzed by a second method whereby at each mixing time a distance is calculated and extrapolated to zero mixing time thereby correcting for spin diffusion (Baleja et al., 1990). The two methods of analysis gave distances which agreed, within experimental error (Table 3). The average distances from the two methods were then utilized in subsequent modeling studies.

Conformation of Enzyme-Bound dTdA in the Presence of Metal Ion. Using the 14 measured (Table 3) and 109 lower-limit interproton distances (based on NOEs which were not observed or determined to be secondary NOEs) together with the five measured and 11 lower-limit Co^{2+}–nucleus distances (Table 2), a structural model of the enzyme-bound dTdA was computed for the D21E mutant enzyme. The distance geometry computation was performed with the program D-Space (Hare Research, Inc.) which takes into account the experimental distances and their errors, the known geometry of all bonds and atoms in dTdA, as well as the van der Waals radii of all atoms of dTdA during the conformational searches. Fifty structures were generated from this program which led to seven acceptable structures that satisfied the experimental distances with a total deviation ≤0.45 Å and with a total van der Waals overlap ≤0.71 Å. Figure 7A shows the structure

Table 3: Interproton Distances (Å) Calculated from NOESY Data of dTdA in the Ternary D21E–La^{3+}–dTdA Complexes of Staphylococcal Nuclease

proton pair B → A[a]	ternary E–metal–dTdA complex		
	method 1 (initial slope)[b]	method 2 (r vs mixing time)[b]	av
TH$_1'$ ↔ TH$_4'$	3.00 ± 0.12	2.98 ± 0.24	2.99 ± 0.27
TH$_1'$ ↔ TH$_2''$[c]	2.37 ± 0.10[c]	2.37 ± 0.10[c]	2.37 ± 0.10[c]
TH$_1'$ ↔ TH$_2'$[d]	2.86 ± 0.20[d]	2.71 ± 0.27[d]	2.78 ± 0.34[d]
AH$_1'$ ↔ AH$_4'$	3.06 ± 0.14	2.90 ± 0.24	2.98 ± 0.28
AH$_1'$ ↔ AH$_5'$H$_5''$	4.13 ± 0.37	4.14 ± 0.37	4.14 ± 0.52
AH$_1'$ ↔ AH$_2''$[c]	2.37 ± 0.10[c]	2.37 ± 0.10[c]	2.37 ± 0.10[c]
AH$_1'$ ↔ AH$_2'$[d]	2.88 ± 0.12[d]	2.94 ± 0.27[d]	2.91 ± 0.30[d]
TH$_6$ ↔ TH$_1'$	2.90 ± 0.34	2.86 ± 0.24	2.88 ± 0.42
TH$_6$ ↔ TH$_5'$H$_5''$	3.42 ± 0.15	3.26 ± 0.15	3.34 ± 0.21
TH$_6$ ↔ TH$_2''$	3.05 ± 0.23	2.99 ± 0.47	3.02 ± 0.52
TH$_6$ ↔ TH$_2'$	2.39 ± 0.10	2.40 ± 0.30	2.40 ± 0.32
TH$_6$ ↔ TCH$_3$	2.77 ± 0.10	2.88 ± 0.28	2.82 ± 0.30
AH$_8$ ↔ AH$_1'$	3.30 ± 0.12	3.22 ± 0.25	3.26 ± 0.28
AH$_8$ ↔ AH$_5'$H$_5''$	3.53 ± 0.25	3.50 ± 0.52	3.52 ± 0.58
AH$_8$ ↔ AH$_2'$	2.53 ± 0.12	2.58 ± 0.27	2.56 ± 0.30
AH$_8$ ↔ AH$_2''$	3.27 ± 0.29	3.40 ± 0.17	3.34 ± 0.34

[a] B ↔ A represents an NOE occurring between protons A and B as measured in both columns and rows of a two-dimensional NOESY. [b] Distances calculated were based on volume integration of the NOESY cross-peaks as described previously (Weber et al., 1991b). [c] Reference distance assumed to be 2.37 ± 0.1 Å based on X-ray data and model building of nucleotides (Ferrin & Mildvan, 1985; Weber et al., 1991b). [d] Expected value is 2.9 ± 0.2 Å based on X-ray data and model building (Rosevear et al., 1983) providing an internal check of the measured interproton distances.

that best fits the data, deviating by 0.44 Å from the measured distances and with a total van der Waals overlap of 0.51 Å. The two most different acceptable structures with a root mean square deviation for all atoms of 1.51 Å are also shown (Figure 7B), illustrating the range of solutions.

The conformational angles and their ranges for dTdA bound to D21E in the presence of metal ions (Figure 7) are tabulated (Table 4) and compared to those found in the same ternary complex of the wild-type enzyme. The glycosidic torsional angles are high-anti for the deoxythymidine residue (58° ≤ χ ≤ 65°) similar to that of wild-type enzyme (64° ≤ χ ≤ 73°) and high-anti for the deoxyadenosine residue (108° ≤ χ ≤ 119°) differing quantitatively from the wild-type enzyme which is also high-anti (66° ≤ χ ≤ 68°). The δ values of 139°–148° for thymidine and 143°–152° for deoxyadenosine (Table 4) indicate both sugars to be predominantly C-2' endo, as also found with the wild-type enzyme. While the angles α, β, and δ of deoxyadenosine and γ, ε, and χ of thymidine are, within error, similar to those of wild-type enzyme, it is clear that in addition to the difference in χ of deoxyadenosine, the angles γ and ζ of thymidine are also very different (Table 4, Figure 1B). Figure 8 compares the most similar acceptable conformations of dTdA on the wild type and on the D21E mutant enzymes showing the differences between them.

Although the kinetic consequences of the change in χ of deoxyadenosine or γ of thymidine are not clear, it is noteworthy that ζ, the dihedral angle about the bond adjacent to the bond being broken, has changed by 124 ± 38° on the D21E mutant (Table 4, Figure 1B). This large structural alteration near the reaction center could, in principle, contribute to the decreased activity of this mutant. To clarify this point, the structure of the metal–dTdA complex determined by NMR was docked into the X-ray structure of the D21E mutant.

Intermolecular Nuclear Overhauser Effects between Enzyme-Bound dTdA and the D21E Mutant of Staphylococcal Nuclease. The aromatic proton resonances of wild-type staphylococcal nuclease in the enzyme–La^{3+}–dTdA complex
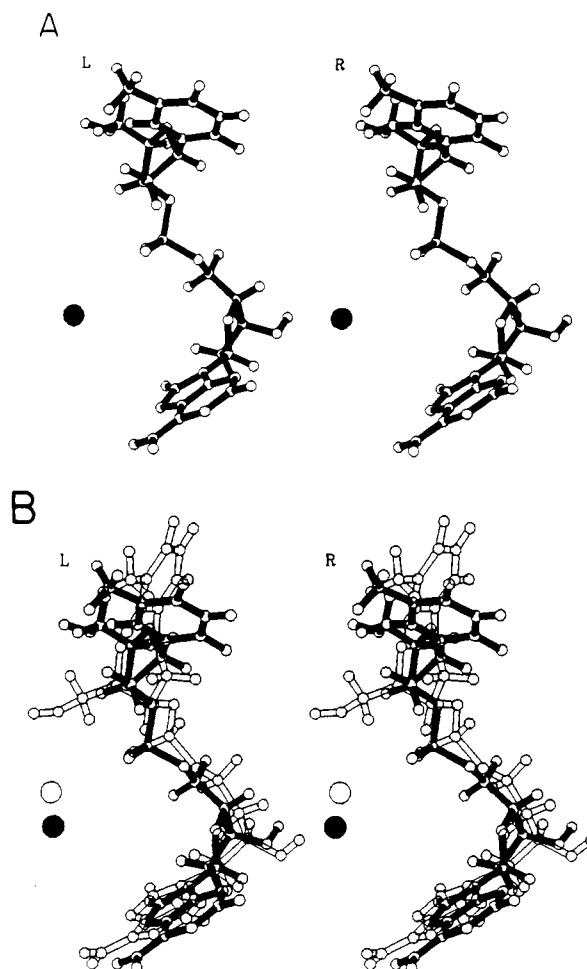
FIGURE 7: Computed conformations of enzyme-bound dTdA in the ternary D21E–metal–dTdA complex based on the experimental distances of Tables 2 and 3. (A) Best fit conformation shown as a stereo pair. (B) Comparison of the two most different acceptable conformations as stereo pairs showing the range of solutions. In B, the root mean square difference between all the atoms of the two limiting structures is 1.51 Å.

Table 4: Comparison of Dihedral Angles (deg) of dTdA in the Enzyme–Metal–dTdA Ternary Complexes of Wild-Type and D21E Mutant of Staphylococcal Nuclease

torsional angle[a]	wild type[b]		D21E mutant[c]	
	dT	dA	dT	dA
α		235 (193–235)		255 (215–255)
β		182 (172–186)		197 (187–277)
γ	53 (33–53)	162 (157–170)	278 (167–279)	161 (152–194)
δ	144 (130–144)	143 (142–143)	140 (139–148)	149 (143–152)
ε	198 (198–205)		195 (195–274)	
ζ	83 (67–83)		207 (201–261)	
χ	64 (64–73)	68 (66–68)	59 (58–65)	117 (108–119)

[a] Torsional angles for α, O$_3'$–P–O$_5'$–C$_5'$; β, P–O$_5'$–C$_5'$–C$_4'$; γ, O$_5'$–C$_5'$–C$_4'$–C$_3'$; δ, C$_5'$–C$_4'$–C$_3'$–O$_3'$; ε, C$_4'$–C$_3'$–O$_3'$–P; ζ, C$_3'$–O$_3'$–P–O$_5'$($_{n+1}$); χ$_{dT}$, O$_4'$–C$_1'$–N$_1$–C$_6$; χ$_{dA}$, O$_4'$–C$_1'$–N$_1'$–C$_8$ (Saenger, 1986; Sundaralingam, 1973; Dickerson et al., 1982; Weber et al., 1991b). [b] Wild-type data have been previously reported (Weber et al., 1991b). [c] The angles were derived from the best acceptable structure with the lowest mean deviations from experimentally measured distances and van der Waals overlap (0.5 Å). The errors reported include the range of acceptable angles in the seven best structures with mean deviations ≤0.5 Å.

have previously been assigned by 2D and 3D NMR studies (Weber et al., 1992). It was previously found that only three aromatic residues, Tyr-85, Tyr-113, and Tyr-115, were near enough to bound dTdA to give intermolecular NOEs to the substrate at short mixing times (Weber et al., 1992). Analysis of the NOESY spectra of the D21E–La^{3+}–dTdA complex at
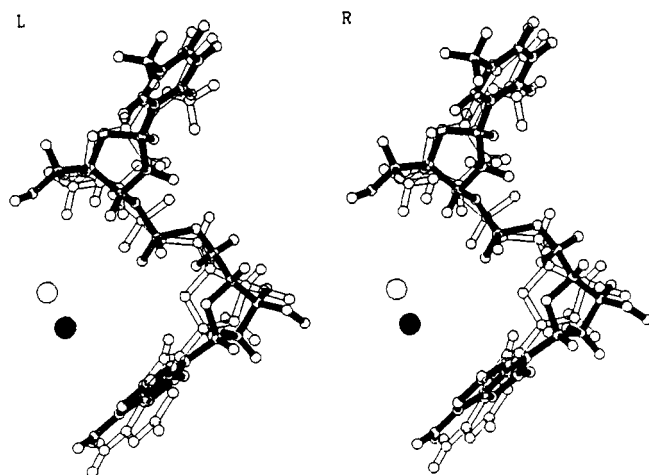
FIGURE 8: Comparison of computed conformations of the enzyme-bound dTdA in the enzyme–metal–dTdA ternary complexes of wild-type (open bonds) and the D21E mutant of staphylococcal nuclease (filled bonds). Shown are the two most similar acceptable conformations as stereo pairs. The root mean square difference between the two structures is 1.24 Å. The conformation of dTdA on the wild-type enzyme was previously reported (Weber et al., 1991b).

mixing times of 50, 100, and 200 ms showed no changes (≤ 0.05 ppm) in the chemical shifts of these tyrosine resonances from those of the wild-type enzyme, with the exception of Tyr-115β which shifted 0.12 ppm upfield and Tyr-115ϵ which shifted 0.13 ppm downfield. Table 5 gives the chemical shifts of the aromatic proton resonances of these tyrosine residues in the ternary D21E complex and assigns the intermolecular NOEs between these residues and the substrate, as observed in the 50-ms NOESY spectra. No other intermolecular NOEs between the aromatic ring protons and the substrate protons were detected at this mixing time. As with the wild-type enzyme, the chemical shifts of the aromatic protons of Tyr-85 and Tyr-113 overlapped, and the ambiguities in the assignments of the NOEs to these residues were clearly resolved by the NMR docking procedure. Also, as with the wild-type enzyme, the D21E mutant gave NOEs only to the dA moiety of dTdA. While eight of the intermolecular NOEs in the ternary D21E–La^{3+}–dTdA complex were also found in the ternary complex of the wild-type enzyme, significant differences in their magnitudes were noted. Qualitative differences between the ternary complex of the wild-type enzyme and the D21E mutant were the loss of NOEs to Tyr-85δ from AH$_4$', to Tyr-85ϵ from AH$_3$', and to Tyr-113ϵ from AH$_8$ (Table 5). New NOEs detected with the D21E mutant were to Tyr-115δ from AH$_2$'', AH$_4$' and from AH$_{5',5''}$ (Table 5). Hence, the precise orientation of the enzyme-bound substrate with respect to these tyrosine residues differs on the D21E mutant.

Docking of Metal–dTdA into the X-ray Structure of D21E Staphylococcal Nuclease. The two most different NMR determined conformations of the metal–dTdA complex (Figure 7B) were each manually docked into the X-ray structure of the D21E·Ca^{2+}–3',5'–pdTp complex, initially by superimposing the metal ions, and subsequently by positioning the dTdA in accord with the intermolecular NOEs between the protons of dTdA and those of Tyr-85, Tyr-113, and Tyr-115 (Table 5). Energy minimization of the ternary complexes were carried out, incorporating the experimental errors in the intramolecular (Tables 2 and 3) and intermolecular distances (Table 5) yielding very similar structures. Initially, 1.5 Å was added to the intermolecular distances to take into account the degeneracies of the δ protons and ϵ protons of the Tyr residues. At later stages of refinement, the assignments of the intermolecular NOEs to specific δ or ϵ protons of each Tyr

residue were easily made. The ambiguities in the NOEs resulting from the overlapping aromatic resonances of Tyr-85 and Tyr-113 were readily resolved by the manual docking procedure, and the assignments of Table 5 were confirmed by the restrained energy minimizations of the manually docked structures which were done to remove residual van der Waals overlaps and to optimize the position of the metal–dTdA complex in accord with the experimental NOEs and distances.

The lowest energy-minimized structure of the D21E–Ca^{2+}–dTdA complex (Figures 1B and 9B), the parameters of which are summarized in Table 6, successfully eliminated the van der Waals overlaps and showed minimal deviations from ideal bond lengths, angles, and planarities, and from the input NOE and metal distance restraints (Tables 2, 3, and 5). On comparing this structure with that of the wild-type enzyme (Figure 1), it is seen that despite the 1.5 Å movement of the metal ion (Libson et al., 1994), the altered conformation of the enzyme-bound substrate (Figure 8), and the differing distances from protons of dTdA to those of Tyr-85, -113, and -115 (Table 5, Figure 9) the catalytic residues Arg-35 and Arg-87 interact with dTdA similarly on the mutant as on the wild-type enzyme. Moreover, on the D21E mutant, the angle of nucleophilic attack on phosphorus defined by the oxygen of an adjacent water ligand of Ca^{2+}, the phosphorus, and the leaving 5'-deoxyadenosyl oxygen of dTdA of 139 ± 17° is consistent with the stereochemical inversion at phosphorus which occurs in the staphylococcal nuclease reaction (Mehdi & Gerlt, 1982) and agrees closely with the value of 131 ± 16° found on the wild-type enzyme (Weber et al., 1992). The reaction coordinate distance from the water oxygen to the attacked phosphorus of 4.8 ± 0.5 Å agrees within error with that found on the wild-type enzyme (4.3 ± 0.5 Å; Weber et al., 1991b, 1992) and is appropriate for an associative nucleophilic displacement at phosphorus (Mildvan, 1981).

DISCUSSION

The three major structural changes at the active site of staphylococcal nuclease resulting from the enlargement of Asp-21 to Glu are an altered position of Ca^{2+}, the direct coordination of Glu-43 by Ca^{2+} as found by X-ray diffraction (Libson et al., 1994), and a distortion of the conformation of the enzyme-bound substrate dTdA as found by NMR (Table 4, Figures 1 and 8). In principle, each of these three changes could contribute to the observed 1500-fold decrease in V_{max}. A change in the position of Ca^{2+} alone, however, may be insufficient to explain a large loss of activity since the enzyme-bound metal ion remains coordinated to the phosphate undergoing nucleophilic attack, and, as previously detected by NMR and EPR (Serpersu et al., 1987, 1988), the metal retains an inner-sphere water ligand, which is well positioned to attack the phosphorus (Figure 1B). Hence, the role of the metal as an electrophile and in promoting catalysis by approximation (Weber et al., 1992) may not be seriously compromised. Accordingly, while both Asp-21 and Asp-40 function as ligands for Ca^{2+} on the wild-type enzyme (Cotton et al., 1979; Loll & Lattman, 1989) only a 12-fold loss in activity is found when Asp-40 is enlarged to Glu (Serpersu et al., 1987). The distortion of the bound substrate, dTdA, in the D21E mutant about the O–P bond adjacent to the bond which is to be cleaved (Figure 1B) might have had a major effect on catalysis, by altering the angle of attack between the entering and leaving groups from the optimal value of 180° expected for inversion (Mehdi & Gerlt, 1982) or by increasing the reaction coordinate distance beyond the value of 4.3 ± 0.5 Å found on the wild-type enzyme (Weber et al., 1991b, 1992).

Table 5: Intermolecular NOEs from Protons of the Enzyme-Bound Substrate dTdA to Tyrosine Protons of the D21E Mutant of Staphylococcal Nuclease in the D21E–La^{3+}–dTdA Complex and Comparison with Wild-Type Enzyme

substrate proton	chemical shift (ppm)	intermolecular NOE to D21E enzyme			intermolecular NOE to wild-type enzyme[a]
		chemical shift (ppm)	magnitude[b]	assignment	magnitude[b]
AH$_8$	8.34	6.73	ND[c]	113ϵ	weak
AH$_2$	8.14	6.63	weak	115ϵ	weak
AH$_{3'}$	4.66	6.73	ND[c]	85ϵ	weak
AH$_{4'}$	4.14	6.73	strong	85ϵ	medium
		6.84	strong	115δ	ND[c]
		6.97	ND[c]	85δ	medium
AH$_{5',5''}$	4.06	6.74	strong	85ϵ	strong
		6.84	medium	115δ	ND[c]
		6.98	strong	85δ	strong
AH$_{2'}$	2.80	6.73	strong	113ϵ	medium
		6.98	strong	113δ	medium
AH$_{2''}$	2.54	6.68	weak	113ϵ	weak
		6.89	weak	115δ	ND[c]
		6.97	weak	113δ	weak

[a] From Weber *et al.*, 1992. [b] Strong, medium, and weak NOEs in the NOESY spectra with a mixing time of 50 ms were assigned values of 2.0–4.5 Å, 2.5–5.0 Å, and 3.0–5.5 Å, respectively. [c] Not detected.
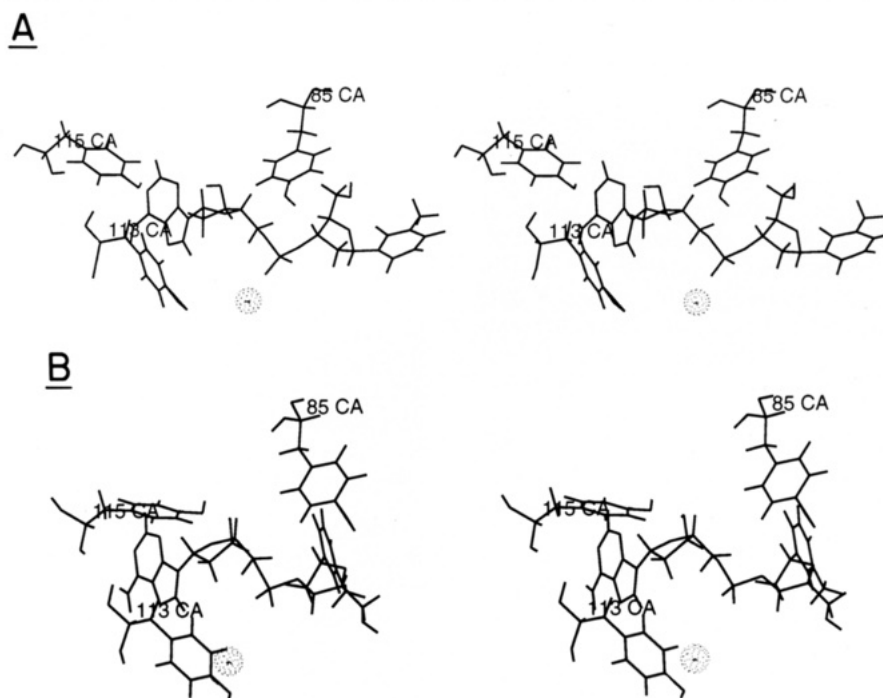

FIGURE 9: Conformation and location of dTdA docked into the X-ray structure of wild type (A) and the D21E mutant of staphylococcal nuclease (B). Also shown are the locations of Tyr-85, Tyr-113, and Tyr-115 which give rise to intermolecular NOEs to the substrate. Ca^{2+} is shown as a stippled sphere.

Table 6: Average Deviations from Ideality and Energies of the Staphylococcal Nuclease D21E–Ca^{2+}–dTdA Docked Structure[a]

potential energy function	
E_{NOE}[b] (kcal/mol)	21.365
E_{vdw}[c] (kcal/mol)	–508.334
deviations from ideality (RMSD)	
bond lengths (Å)	0.01
bond angles (deg)	2.42
impropers[d] (deg)	0.18

[a] The restrained energy minimization resulted in small changes in the backbone (0.48 Å RMSD) and side chain atoms (0.90 Å RMSD) from the X-ray structure of the D21E enzyme. [b] Utilizing the force constant 30 kcal/mol/Å^2. [c] Utilizing the CHARMM parameters (Brooks *et al.*, 1983) for the Lennard-Jones potential. [d] Deviations from planarity in aromatic ring systems and peptide bonds.

Apparently, however, these effects did not occur. Thus, the NMR-docked structure showed an angle of attack of 139 ± 17°, comparable to the value of 131 ± 16° found on the wild-type enzyme (Weber *et al.*, 1992), and the reaction coordinate

distance of 4.8 ± 0.5 Å on the D21E mutant overlapped with that found on the wild-type enzyme.

Hence, the most damaging effect on catalysis may result from the direct coordination of Glu-43 by Ca^{2+}, making it at least temporarily unavailable to assist in catalysis. The role of Glu-43, originally proposed as a general base involved in deprotonating the attacking water, was based on its location as a hydrogen bond acceptor from a water ligand, both in the crystal (Cotton *et al.*, 1979; Loll & Lattman, 1989) and in the NMR-docked structures (Figure 1A, Weber *et al.*, 1992) and on the observation that the E43S mutation results in a 2700-fold loss in V_{max} which is partially restored by increasing the pH (Serpersu *et al.*, 1989). Other mutations of Glu-43 to Asp, Asn, Gln, and Ala result in 10^2- to 10^4-fold decreases in V_{max}, in some cases comparable to the effects of the D21E mutation (Hibler *et al.*, 1987). Further evidence consistent with a direct role of Glu-43 in catalysis is the observation that its effects on V_{max} are, in part, cooperative with those of the likely acid catalyst Arg-87, as found by the partially additive

effects on V_{max} of the E43S and R87G single mutations in the E43S + R87G double mutant (Weber *et al.*, 1991a).

The proposed role of Glu-43 as a general base has recently been questioned based on the increase in V_{max} with pH well beyond the expected pK_A value of Glu-43 (Hale *et al.*, 1993) indicating specific base catalysis or direct attack by OH^-. However, such effects of OH^- do not exclude simultaneous general base catalysis by Glu-43. Direct evidence for general base catalysis by Glu-43 cannot be easily obtained by pH–rate studies due to the extremely low activity of staphylococcal nuclease below pH 5.5 (Hale *et al.*, 1993).

Further evidence against the role of Glu-43 as a general base was provided by the observation that V_{max} decreased by only 24-fold at pH 7.5 on replacing Glu-43 with an isosteric, isoelectronic, but weakly basic residue containing a nitroalkane side chain (Judice *et al.*, 1993). Although nitroalkane groups are very weak bases, they can function as hydrogen bond acceptors (Rao, 1964). However, deprotonation of the carbon bearing the nitro group ($9.0 \leq pK_A \leq 10.8$; Porter & Bright, 1980; Schloss *et al.*, 1980) yields bases stronger than glutamate ($pK \sim 4$). While such bases are very slow in binding and dissociating protons on carbon, the nitroanion resonance form could rapidly and reversibly accept a proton on the negatively charged oxygens and could thereby function as a general base. Despite this possibility, a different role for Glu-43 has been proposed as adjusting the geometry of the Ω loop consisting of residues 43–52, fixing it into an optimal position for catalysis (Hale *et al.*, 1993; Judice *et al.*, 1993). However, deletion of six of the 10 residues of this loop (residues 44–49), converting it to a type II' β turn, results in only a 40-fold decrease in V_{max} (Poole *et al.*, 1991; Baldisseri *et al.*, 1991), casting doubt on the importance of most of this loop to catalysis. Hence, Glu-43 may function as a general base, as originally proposed (Cotton *et al.*, 1979; Hibler *et al.*, 1987; Serpersu *et al.*, 1989).

An alternative role for Glu-43, consistent with all of the above observations, which also makes use of its observed hydrogen-bonded proximity to a coordinated water on the Ca^{2+} is that its carboxylate group orients and holds a hydroxyl ligand of Ca^{2+} in an optimal position to attack the phosphodiester phosphorus. Conversion of a water ligand to a hydroxyl could be accomplished either by specific base catalysis or by ligand substitution of an inner sphere water by a hydroxyl ion from the second coordination sphere. Also consistent with this hypothesis is the observation of an aquo ligand on Ca^{2+} by X-ray crystallography on the wild-type enzyme where it is hydrogen bonded by Glu-43 (Loll & Lattman, 1989) and its absence, due to low occupancy, on the D21E mutant (Libson *et al.*, 1994). Water ligands on Ca^{2+}, dissociate very rapidly (10^8 s^{-1}; Eigen & Hammes, 1963), a process which would be significantly slowed by hydrogen bonding, and aliphatic nitro groups can function as hydrogen bond acceptors (Rao, 1969). A role for Glu-43 in orienting the attacking hydroxyl ligand would also be consistent with its cooperativity with Arg-87 in promoting catalysis (Weber *et al.*, 1991a).

REFERENCES

Anfinsen, C. B., Cuatrecasas, P., & Taniuchi, H. (1971) *Enzymes* (*3rd ed.*) *4*, 177–204.

Baldisseri, D. M., Torchia, D. M., Poole, L. B., & Gerlt, J. A. (1991) *Biochemistry 30*, 3628–3633.

Baleja, J. D., Moult, J., & Sykes, B. D. (1990) *J. Magn. Reson. 87*, 375–384.

Bean, B. L., Koren, R., & Mildvan, A. S. (1977) *Biochemistry 16*, 3322–3333.

Bradford, M. M. (1976) *Anal. Biochem. 72*, 248–254.

Brooks, R. R., Bruccoleri, R. E., Olafson, B. D., States, D. J., Swaminathan, S., & Karplus, M. J. (1983) *J. Comput. Chem. 4*, 187–217.

Brünger, A. T. (1990) XPLOR Manual, Version 2.1, Yale University, New Haven, CT.

Carr, H. Y., & Purcell, E. M. (1954) *Phys. Rev. 94*, 630–638.

Chuang, W. J., Weber, D. J., Gittis, A. G., & Mildvan, A. S. (1993) *Proteins: Struct., Funct., Genet. 17*, 36–48.

Cohn, M. S., & Townsend, J. (1954) *Nature (London) 173*, 1090–1091.

Cotton, F. A., Hazen, E. E., Jr., & Legg, M. J. (1979) *Proc. Natl. Acad. Sci. U.S.A. 76*, 2551–2555.

Cuatrecasas, P., Fuchs, S., & Anfinsen, C. B. (1967a) *J. Biol. Chem. 242*, 1541–1547.

Cuatrecasas, P., Fuchs, S., & Anfinsen, C. B. (1967b) *J. Biol. Chem. 242*, 3063–3067.

Dickerson, R. E., Drew, H. R., Conner, B. N., Wing, R. M., Frantini, A. V., & Kopka, M. L. (1982) *Science 216*, 475–485.

Dunn, B. M., DiBello, C., & Anfinsen, C. B. (1973) *J. Biol. Chem. 248*, 4769–4774.

Eigen, M., & Hammes, G. G. (1963) *Adv. Enzymol. 25*, 1–38.

Ferrin, L. J., & Mildvan, A. S. (1985) *Biochemistry 24*, 6904–6913.

Fry, D. C., Kuby, S. A., & Mildvan, A. S. (1985) *Biochemistry 24*, 4680–4694.

Hale, S. P., Poole, L. B., & Gerlt, J. A. (1993) *Biochemistry 32*, 7479–7487.

Hibler, D. W., Stolowich, J. M., Reynolds, M. A., Gerlt, J. A., Wilde, J. A., & Bolton, P. H. (1987) *Biochemistry 26*, 6278–6286.

Jeener, J., Meier, B. H., Bachmann, P., & Ernst, R. R. (1979) *J. Chem. Physics 71*, 4546–4553.

Judice, J. K., Gamble, T. R., Murphy, E. C., deVos, A. M., & Schultz, P. G. (1993) *Science 261*, 1578–1581.

Kumar, A., Wagner, G., Ernst, R. R., & Wüthrich, K. (1980) *Biochem. Biophys. Res. Commun. 96*, 1156–1163.

Libson, A. M., Gittis, A. G., & Lattman, E. E. (1994) *Biochemistry* (preceding paper in this issue).

Loll, P., & Lattman, E. E. (1989) *Proteins: Struct., Funct., Genet. 5*, 183–201.

Marion, D., & Wüthrich, K. (1983) *Biochem. Biophys. Res. Commun. 113*, 967–974.

Mehdi, S., & Gerlt, J. A. (1982) *J. Am. Chem. Soc. 104*, 3223–3225.

Mildvan, A. S. (1981) *Phil. Trans. Roy. Soc. London, Ser B. 293*, 65–74.

Mildvan, A. S., & Engle, J. L. (1972) *Methods Enzymol. 26C*, 654–682.

Mildvan, A. S., & Gupta, R. K. (1978) *Methods Enzymol. 49G*, 322–359.

Mildvan, A. S., & Serpersu, E. H. (1989) in *Metal Ions in Biological Systems* (Sigel, H., ed.) Vol. 25, pp 309–334, Marcel Dekker, Inc., New York.

Mildvan, A. S., Granot, J., Smith, G. M., & Liebman, M. (1979) *Adv. Inorg. Biochem. 2*, 211–236.

Poole, L. B., Loveys, D. A., Hale, S. P., Gerlt, J. A., Stanczyk, S. M., & Bolton, P. H. (1991) *Biochemistry 30*, 3621–3627.

Porter, D. J. T., & Bright, H. J. (1980) *J. Biol. Chem. 255*, 4772–4780.

Pourmotabbed, T., Dell'Acqua, M., Gerlt, J. A., Stanczyk, S. M., & Bolton, P. H. (1991) *Biochemistry 29*, 3677–3683.

Rao, C. N. R. (1969) in *The Chemistry of the Nitro and Nitroso Groups* (Feuer, H., Ed.) Part 1, 112–116, Interscience, New York.

Reed, G. H., Cohn, M., & O'Sullivan, W. J. (1970) *J. Biol. Chem. 245*, 6547–6552.

Rosevear, P. R. Bramson, H. N., O'Brian, C., Kaiser, E. T., & Mildvan, A. S. (1983) *Biochemistry 22*, 3439–3447.

Sack, J. S. (1988) *J. Mol. Graphics 6*, 224–225.

Saenger, W. (1986) *Principles of Nucleic Acid Structure*, Springer-Verlag, New York.

Schloss, J. V., Porter, D. J. T., Bright, H. J., & Cleland, W. W. (1980) *Biochemistry 19*, 2358–2362.

Serpersu, E. H., Shortle, D. R., & Mildvan, A. S. (1986) *Biochemistry 25*, 68–77.

Serpersu, E. H., Shortle, D., & Mildvan, A. S. (1987) *Biochemistry 26*, 1289–1300.

Serpersu, E. H., McCraken, J., Peisach, J., & Mildvan, A. S. (1988) *Biochemistry 27*, 8034–8044.

Serpersu, E. H., Hibler, D. W., Gerlt, J. A., & Mildvan, A. S. (1989) *Biochemistry 28*, 1539–1548.

Shortle, D., & Lin, B. (1985) *Genetics 110*, 539–555.

Sundaralingam, M. (1973) *Jerusalem Symp. Quant. Chem. Biochem. 5*, 417–456.

Torchia, D. A., Sparks, S. W., & Bax, A. (1989) *Biochemistry 28*, 5509–5524.

Tucker, P. W., Hazen, E. E., Jr., & Cotton, F. A. (1978) *Mol. Cell. Biochem. 23*, 67–86.

Tucker, P. W., Hazen, E. E., Jr., & Cotton, F. A. (1979) *Mol. Cell. Biochem. 23*, 3–16.

Wang, J., LeMaster, D. M., & Markley, J. L. (1990) *Biochemistry 29*, 88–101.

Weber, D. J., Serpersu, E. H., Shortle, D., & Mildvan, A. S. (1990) *Biochemistry 29*, 8632–8642.

Weber, D. J., Meeker, A. K., & Mildvan, A. S. (1991a) *Biochemistry 30*, 6103–6114.

Weber, D. J., Mullen, G. P., & Mildvan, A. S. (1991b) *Biochemistry 30*, 7425–7437.

Weber, D. J., Gittis, A. G., Mullen, G. P., Abeygunawardana, C., Lattman, E. E., & Mildvan, A. S. (1992) *Proteins: Struct., Funct., Genet. 13*, 275–287.

Weber, D. J., Serpersu, E. H., Gittis, A. G., Lattman, E. E., & Mildvan, A. S. (1993) *Proteins: Struct., Funct., Genet. 17*, 20–35.

Weber, D. J., Libson, A. M., Gittis, A. G., Lebowitz, M. S., & Mildvan, A. S. (1994) Abstr. ASBMB Mtg. Washington, D.C., *FASEB. J. 8*, A1278.

Wüthrich, K. (1986) *NMR of Protons and Nucleic Acids*, John Wiley, New York.